Journal of Cleaner Production 465 (2024) 142840

Contents lists available at ScienceDirect

Journal of Cleaner Production

journal homepage: www.elsevier.com/locate/jclepro

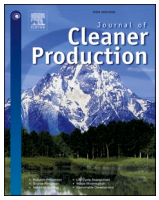

A generic approach for modelling hydrogen-methane-air detonation in hydrocode

Di Chen [a], Jun Li [a,*], Li Wang [b,**], Chengqing Wu [a]

[a] School of Civil and Environmental Engineering, University of Technology Sydney, Sydney, NSW, 2007, Australia
[b] Tianjin Chengjian University, Tianjin, 300384, China

ARTICLE INFO

Handling Editor: Panos Seferlis

Keywords:
Gas detonation
Numerical modelling
Loading prediction
Hydrogen-methane-air

ABSTRACT

Hydrogen is pivotal in the transition to a sustainable energy supply. The presence of hydrogen-methane mixtures is increasing as the feasibility of utilizing existing natural gas infrastructure for large-scale hydrogen transportation and distribution. However, recent explosion accidents underscore the need to understand the detonation hazards of hydrogen and methane. Current modelling techniques for hydrogen-methane-air detonations are computationally prohibitive due to extra-fine mesh and time step requirements to solve the chemical reaction coupling within detonation structure. This study presented a generic approach to address these challenges, enabling precise and rapid simulation of hydrogen-methane-air blast profiles within hydrocodes. Modified open-source codes helped bypass the time-consuming implicit coupling of detailed chemical reactions with detonation structure and thermodynamic properties based on Chapman-Jouguet (C-J) theory and equilibrium reactive flow assumption, yielding a 90% reduction in computational time. An empirical model, developed through theoretic calculations, provided C-J parameters for hydrocode input with high accuracy across typical industrial conditions. Then, these C-J parameters were employed in LS-DYNA hydrocode based on modified Jones-Wilkins-Lee (JWL) equation of state (EoS) to simulate the hydrogen-methane-air blast loading. This approach was validated against diverse experimental data, encompassing hydrogen-air, methane-air, and hydrogen-methane-air mixtures, and various fuel concentrations, experimental scales, confinement conditions, and fuel shapes. Although conservative results were observed in unstable detonations near the lower detonable limit, it outperformed traditional CFD methods in both accuracy and efficiency. Furthermore, the use of hydrocodes enables the analysis of blast loading as well as the dynamic behaviour of structures subjected to explosive forces. This approach is easily adaptable to other gaseous detonations beyond hydrogen-methane-air by simply replacing the chemical reaction models, making it a versatile tool across various fields.

1. Introduction

Hydrogen and natural gas play a crucial role in the transition towards a sustainable energy supply. The Hydrogen Council predicts that 18% of energy demand will be provided by hydrogen by 2050 (Hydrogen scaling up, 2017). Natural gas, primarily composed of methane, accounts for 24% of global primary energy in 2022 (Institute, 2023). Methane and hydrogen can be stored, transported, and utilized individually or as a blend. Demonstrations have shown the feasibility of blending hydrogen with natural gas, leveraging existing infrastructure for large-scale hydrogen transportation and distribution (Chae et al., 2022), thereby increasing the likelihood of methane-hydrogen mixtures in daily life.

Despite their potential, both methane and hydrogen are highly flammable gases, posing risks of explosion accidents with severe consequences. Notable gas explosion accidents in Qingdao (Zhu et al., 2015) and Kaohsiung (Yang et al., 2016), and South Korea in 2019 (Kim et al., 2023), underscore the urgency of understanding and managing the safety aspects associated with these gases. As shown in Table 1, methane and hydrogen exhibit different combustion and explosion characteristics, necessitating careful consideration of these differences when handling and utilizing them and their mixtures.

To develop resilient structures capable of withstanding blasts, a comprehensive understanding of structural reactions subjected to

* Corresponding author.
** Corresponding author.
E-mail addresses: jun.li-2@uts.edu.au (J. Li), wangli@tcu.edu.cn (L. Wang).

https://doi.org/10.1016/j.jclepro.2024.142840
Received 7 February 2024; Received in revised form 26 May 2024; Accepted 8 June 2024
Available online 10 June 2024

Table 1
Combustion and explosion characteristics for methane/hydrogen.

Property	H_2	CH_4
Flammable range	4–75 %	4.3–15 %
Ignition energy	0.02 mJ	0.28 mJ
Autoignition temperature	520 °C	540 °C
Laminar Flame Speed	28 m/s	3.5 m/s
Self-ignition	Likely when release from high-pressure container	unlikely
Detonation level	18.3%–59%	unlikely

methane/hydrogen explosion is essential (Hao et al., 2016). Gas explosions can be categorized into deflagration and detonation based on the relative speed of the flame front and shock head, with detonation being the most destructive form (Bjerketvedt et al., 1997). Blast loading is intricately coupled with structural configuration and response, especially in close-in blast loading scenarios. Consequently, it is imperative to concurrently address blast loading and structural response.

Precisely capturing the structural response to gas explosions presents substantial challenges. Experimental testing is often impractical due to its costly and hazardous nature (Chen et al., 2022, 2023a; Li et al., 2021; Xing et al., 2020; Sun et al., 2020; Jin et al., 2021; Liao et al., 2023). Conversely, numerical simulation grapples with computational efficiency challenges arising from the coupling of chemical reactions, fluid dynamics, and structural deformation (Chen et al., 2023b). While the energy equivalent method has been widely used, replacing the gas explosion source with an equivalent high explosive, it is deemed inappropriate for near-field scenarios owing to the significantly different energy release rates (Kim et al., 2023; van den Berg, 1985; López et al., 2015; Guo et al., 2016; Zhang et al., 2015; Zhang et al., 2014; Van den Berg et al., 1993), as high explosives having much greater energy release rate as compared to gas explosion sources (Hao et al., 2016). Pure Computational Fluid Dynamics (CFD) tools (Yáñez et al., 2011a), such as FLUENT (Machniewski et al., 2022), FLACS (Zhang et al., 2020), OPENFOAM (Kim et al., 2019), etc., primarily focus on blast loads, while assuming rigid structures, leading to notable discrepancies in load prediction when significant structural deformation occurs. Meanwhile, CFD tools with fluid-structural interaction capabilities often fail to consider strain rate effects on materials under dynamic loading (Li et al., 2019; Baker et al., 2010).

Hydrocodes are specialized computer programs designed to address the highly dynamic behaviour of structures subjected to explosive loading (Anderson, 1987; Pan et al., 2023, 2024). Utilizing high-rate continuum modelling, these tools directly capture both blast profiles and structural responses (Baker et al., 2010). LS-DYNA stands out as one of the most extensively utilized hydrocodes for addressing high strain rate problems induced by blast loading (Hao et al., 2016). Initially focused on high explosives like TNT, LS-DYNA recently developed a chemistry solver to simulate reactive flows and structural responses. This coupling has proven adequate in accurately capturing blast loading for near- and far-field hydrogen detonations (Chen et al., 2023b). However, limitations remain from solving the intricate chemical reactions consumes a remarkable portion (60%–70%) of computational resources, even with simplified chemical reaction models (Chen et al., 2023b). This issue becomes even more pronounced for methane-air combustion due to its more complex reaction mechanisms. Additionally, denoting gas detonation front requires fine mesh resolutions on the order of millimeters, impractical for large-scale scenarios (Bozier et al., 2009; GROETHE et al., 2007).

This study aimed to develop an accurate and computationally efficient method for the modelling of blast profiles for CH_4–H_2-air detonations within hydrocode. Classical detonation theory suggests that a stable detonation front propagates at constant velocity and pressure (Bozier et al., 2009), which allows to leverage external tools and equilibrium Chapman-Jouguet (C-J) theory to approximate properties within the detonation front, avoiding the need of complex meshing and chemical-fluid coupling, signally reducing computational cost. A modified Jones-Wilkins-Lee (JWL) equation of state was employed to model the detonation process inside the gas-air mixture. The proposed method was validated against diverse experimental conditions and compared with traditional CFD methods to demonstrate its accuracy and computational efficiency for large-scale scenarios.

2. Methodology

2.1. Evaluating equilibrium C-J parameters

2.1.1. Conservative equations for reacting compressible flow

The fluid and chemistry are strongly coupled in the gas detonation front, and the field equations describing mass, momentum, energy and species transport for a reacting compressible flow in a control volume in conservation form can be written as Equation (1) to Equation (4) (Kao et al., 2023):

$$\frac{\partial \rho}{\partial t} + \nabla\cdot(\rho \mathbf{u}) = 0 \qquad \text{Equation 1}$$

$$\frac{\partial \rho \mathbf{u}}{\partial t} + \nabla\cdot(\rho \mathbf{u}\mathbf{u}) = -\nabla P + \nabla\cdot\tau \qquad \text{Equation 2}$$

$$\frac{\partial}{\partial t}\left(e + |\mathbf{u}|^2 \Big/ 2\right) + \nabla\cdot\left[\rho\mathbf{u}\left(h + |\mathbf{u}|^2 \Big/ 2\right)\right] = -\nabla\cdot\mathbf{q} + \nabla\cdot(\tau\cdot\mathbf{u}) \qquad \text{Equation 3}$$

$$\frac{\partial \rho Y_k}{\partial t} + \nabla\cdot(\rho \mathbf{u} Y_k) = -\nabla\cdot\mathbf{j}_k + \dot{\Omega}_k \quad k = 1, 2, \ldots, K \qquad \text{Equation 4}$$

where ρ is the mass density, kg/m^3; P is the pressure, Pa; $\mathbf{u}$ denotes the velocity vector, m/s; $h = e + P/\rho$ represents the enthalpy, J/kg; e is the internal energy, J/kg; Y_k is the mass fraction of k-th species; $\dot{\Omega}_k = \mathscr{W}_k\dot{\omega}_k$ denotes the net species production rate, kg/(m^3. s), which is computed by detailed chemical kinetics, and $\mathscr{W}_k$ is the mole mass of k-th species, kg/mol, and $\dot{\omega}_k$ denotes the net molar production rate, mol/(m^3. s); τ represents the viscous stress tensor, Pa; $\mathbf{j}_k$ is the species mass diffusion flux, kg/(m^2. s); $\mathbf{q}$ is the thermal energy flux. An equation of state (EoS) is required to complete Equation (1) to Equation (4). In this study, both the reactants and products are considered as ideal gas (Kao et al., 2023). The reason for using ideal gas assumption for gas detonation will be explained in the latter section.

The actual gas detonation front exhibits a complex three-dimensional structure consisting of intricate cellular patterns (Rudy et al., 2016; Stamps et al., 2006). Accurately capturing this structure demands extremely high mesh resolution, which can become computationally prohibitive for large-scale scenarios, particularly when coupled with detailed chemical reaction models. However, this study aims to provide a computationally efficient approach for modelling gas detonations in the context of typical industrial accidents. Therefore, we focus on the overall detonation wave propagation rather than the uneven pressure distribution within the detonation front, which represents a thin layer as compared to the entire flow field. Consequently, as highlighted in C-J theory by Chapman and Jouguet (Chapman, 1899; Jouguet, 1905), the detailed detonation structure was simplified as a strong discontinuity with no thickness between the unburnt and burnt fuel, propagating at a steady, characteristic speed specific to the gas mixture. Other assumptions based on C-J theory include: (1) the viscosity in the up and down stream of the shock was ignored; (2) the flow was adiabatic and one-dimensional quasi-steady; (3) the chemical reaction in the shock front is assumed to happen instantly to reach an equilibrium flow. Therefore, the species in the shock front react infinitely fast and the composition shifts to match the local thermodynamics state, $\mathbf{Y}$=$\mathbf{Y}_{eq}$ (P, T).

With these simplifications, as shown in Fig. 1, for a detonation wave

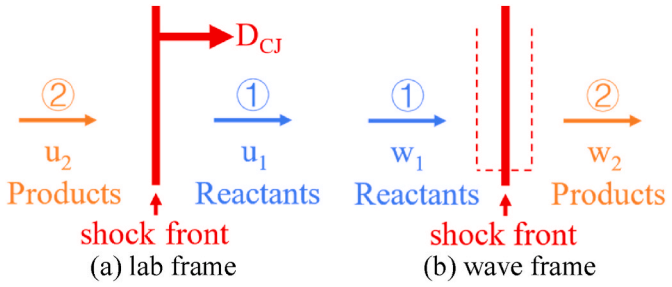

Fig. 1. The transformation from the laboratory to the wave fixed reference frame.

propagating at a speed of D_{cj} (the ground as the reference frame, m/s) into the unburnt fuel mixture at state 1 which has a moving speed of u_1 (the ground as the reference frame, m/s), the lab frame reference (Fig. 1 (a)) can be transformed into a stationary wave (Fig. 1 (b)) with an upstream flow speed w_1 (m/s) and a downstream flow speed w_2 (m/s), where

$$w_1 = D_{CJ} - u_1 \quad \text{Equation 5}$$

$$w_2 = D_{CJ} - u_2 \quad \text{Equation 6}$$

For most gas explosion accidents, $D_{CJ} \gg u_1$. Therefore, u_1 can be ignored, and $w_1 = D_{CJ}$. In this study, chemical reactions were included, and an equilibrium condition was assumed after the shock front. As the coordinate system is established on the wave front, only the velocity components normal to the detonation front need to be considered, resulting in the conservative equations for the equilibrium reaction:

$$\rho_1 w_1 = \rho_2 w_2 \quad \text{Equation 7}$$

$$P_1 + \rho_1 w_1^2 = P_2 + \rho_2 w_2^2 \quad \text{Equation 8}$$

$$\rho_1 w_1 U_1 + P_1 w_1 + \frac{1}{2}\rho_1 w_1 \cdot {w_1}^2 = \rho_2 w_2 U_2 + P_2 w_2 + \frac{1}{2}\rho_2 w_2 \cdot {w_2}^2 \quad \text{Equation 9}$$

where Equation (7) to Equation (9) are the conservative equation of mass, momentum, and energy, respectively. Parameters with subscript 1 indicate the condition in reactants (unburnt), while with subscript 2 imply the condition in the equilibrium products. P denotes absolute pressure, Pa; ρ represents density, kg/m^3; U is the total internal energy per unit mass, J/kg, including state internal energy e (J/kg) and chemical energy Q (J/kg), and the total internal energy in the reactants and products can be calculated by Equation (10).

$$\left.\begin{aligned} U_1 &= e_1 + Q_1 \\ U_2 &= e_2 + Q_2 \end{aligned}\right\} \quad \text{Equation 10}$$

From Equation (7) and Equation (8), the following two equations can be obtained:

$$D_{CJ} = v_1\sqrt{\frac{P_2 - P_1}{v_1 - v_2}} \quad \text{Equation 11}$$

$$u_2 = (v_1 - v_2)\sqrt{\frac{P_2 - P_1}{v_1 - v_2}} \quad \text{Equation 12}$$

where v is the relative volume which equals to $1/\rho$, m^3/kg. By combining Equation (9) to Equation (12), the detonation energy release $Q_{CJ\text{-}M}$ can be calculated by Equation (13):

$$Q_{CJ-M} = Q_2 - Q_1 = e_2 - e_1 + \frac{1}{2}(P_2 + P_1)(v_2 - v_1) \quad \text{Equation 13}$$

where $Q_{CJ\text{-}M}$ has the unit of J/kg; e is the internal energy related to state, J/kg, which is related to the components and temperature of gas mixture.

2.1.2. Thermodynamic property representation

Thermodynamic properties, such as internal energy, enthalpy, entropy, etc., were fundamental to the flow and chemical calculation. For ideal gas mixtures, the thermodynamic properties are determined by the composition, molar properties of each species, and the state (pressure, temperature) of the mixture (Kao et al., 2023). The thermodynamic properties for ideal gas mixtures can be derived from three basic thermodynamic properties: c_p/R, h/RT, and s/R for each species, which were evaluated as a function of temperature using the NASA-7 style polynomials.

$$\frac{c_p(T)}{R} = \begin{cases} \sum_{n=0}^{4} a_n T^n & T_{min} \le T \le T_{mid} \\ \sum_{n=0}^{4} b_n T^n & T_{mid} \le T \le T_{max} \end{cases} \quad \text{Equation 14}$$

$$\frac{h(T)}{RT} = \begin{cases} \sum_{n=0}^{4} \frac{a_n T^n}{n+1} + \frac{a_5}{T} & T_{min} \le T \le T_{mid} \\ \sum_{n=0}^{4} \frac{b_n T^n}{n+1} + \frac{b_5}{T} & T_{mid} \le T \le T_{max} \end{cases} \quad \text{Equation 15}$$

$$\frac{s(T)}{R} = a_0 \ln T + a_1 T + \frac{a_2}{2}T^2 + \frac{a_3}{3}T^3 + \frac{a_4}{4}T^4 + a_6 \quad \text{Equation 16}$$

where c_p denotes the heat capacity per unit mass at constant pressure, J/(kg.K); a_0 to a_6 are the coefficients of the polynomial for each species; h is the enthalpy per unit mass, J/(kg.K); s represents entropy per unit mass, J/(kg.K). In this study, two pairs of polynomials were employed to cover the low-temperature (200–1000 K) and high-temperature ranges (1000–6000 K) to make sure the thermodynamic properties were presented properly in the detonation front (Mcbride et al., 1993), e.g., T_{min} = 200 K; T_{mid} = 1000 K, and T_{max} = 6000 K.

2.1.3. The ideal gas assumption

An ideal gas model simplifies the analysis of detonation mixtures by ignoring two key factors: (1) the influence of intermolecular forces, and (2) the finite size of atoms and molecules (Weng et al., 2022). This assumption allows for universal EoS applicable to all reactants and products, eliminating the need for individual EoS development for each species under varying temperature and pressure conditions. Consequently, this approach significantly simplifies the evaluation of thermodynamic properties for the detonation mixture.

The ideal gas assumption is effective, especially in low pressure and high temperature. Quantified analysis reveals that for H_2–O_2 mixture at room temperature and 7 MPa initial pressure, the ideal gas assumption only underestimated the C-J pressure by 2% in comparison with experiment results when the C-J pressure is approximately 100 MPa (Weng et al., 2022). In the case of gaseous explosives in room conditions, the detonation pressures are considerably lower. For example, C-J pressures are approximately 1.58 MPa, 1.74 MPa, and 1.86 MPa for H_2-air, methane-air, and ethylene-air mixtures (Bjerketvedt et al., 1997), respectively, under room conditions. Therefore, the ideal gas assumption for gaseous explosives under room condition should offer enough accuracy for industrial accident modelling.

2.1.4. Procedure to calculate C-J parameters

This section describes the procedure used to calculate the C-J parameters (thermodynamic properties and detonation velocity) for H_2–CH_4-air mixtures at specified initial states (temperature, pressure, and composition). These parameters serve as inputs for hydrocode simulations to model gas detonation processes and their impact on structures.

The energy release and species transport within the mixture under C-J conditions are simulated using the GRI-Mech 3.0 detailed chemical reaction mechanism (Smith, 2000). Originally developed for CH_4 combustion, this mechanism consists of 53 species and 325 reactions. While designed for natural gas combustion, its detailed combustion reaction mechanism for hydrogen renders it well-suited for accurately modelling the detonation process in H_2–CH_4-air mixtures (Bozier et al., 2009; WANG et al., 2009).

Because the equilibrium composition is strongly coupled with the C-J pressure, temperature which is implicitly contained with compositions, there are no analytical solutions for equilibrium C-J parameters. Consequently, an iterative technique is required to solve this implicit problem using Newton-Raphson method (Kao et al., 2023). The procedure to evaluate equilibrium C-J parameters is present in Fig. 2. The first step is to determine the C-J detonation velocity based on an iterative process of guessing detonation velocity ρ_2 and detonation temperature T_2, and the stable detonation velocity is the minimum wave speed which can be inferred from the C-J theory (Kao et al., 2023). The equilibrium composition is determined based on the minimum Gibbs energy theory (Gordon and McBride, 1994). Once the detonation velocity, equilibrium composition and T_2 are determined, other thermodynamic properties are calculated based on Equation (7) to Equation (13). This procedure was achieved in a MATLAB environment by utilizing the open-source Cantera library (Goodwin et al., 2023) and Shock and Detonation Toolbox (Kao et al., 2023).

2.2. Employing C-J parameters in hydrocode

To model the gas detonation by employing the C-J parameters, a constitutive model was required to represent the gas-air mixture. The *MAT-HIGH_EXPLOSIVE_BURN material model, coupled with the *EOS_JWL equation of state model in the LS-DYNA hydrocode, was chosen to model the gas detonation process.

The JWL equation of state underwent a specific modification to model gas detonation under the ideal gas assumption. The form of JWL equation is presented in Equation (17) (Lee et al., 1968), as the pressure decreases, the contributions of the first and second terms in the JWL equation diminish, and the third term dominates the total pressure. E.g., as shown in Fig. 3, for Composition B, Grade A, the third term in the JWL equation becomes the predominant pressure contributor after the total pressure drops to approximately 75 MPa or less (LS-DYNA® Keyword User, 2021), resembling the behaviour of an ideal gas equation. Consequently, the parameters A and B in Equation (17) were set to 0, and R_1 and R_2 were set to 1 to prevent division by zero. The ω in the third term equals to γ_{CJ}-1, where γ_{CJ} was introduced in the later part.

$$p = A\left(1 - \frac{\omega}{R_1 V}\right)e^{-R_1 V} + B\left(1 - \frac{\omega}{R_2 V}\right)e^{-R_2 V} + \frac{\omega E}{V} \qquad \text{Equation 17}$$

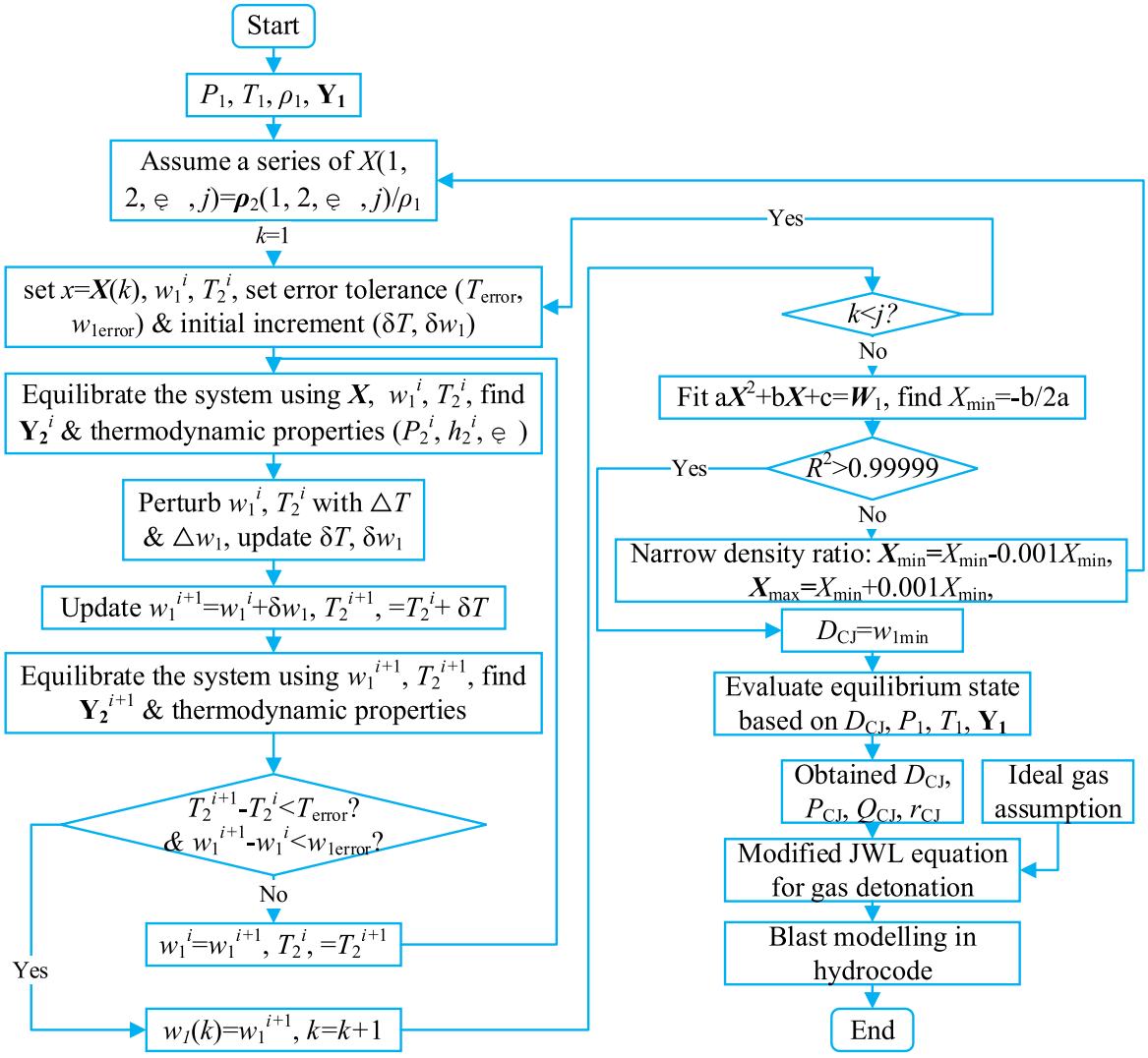

Fig. 2. Flow chart of the modelling of CH_4–H_2-air detonation in hydrocode.

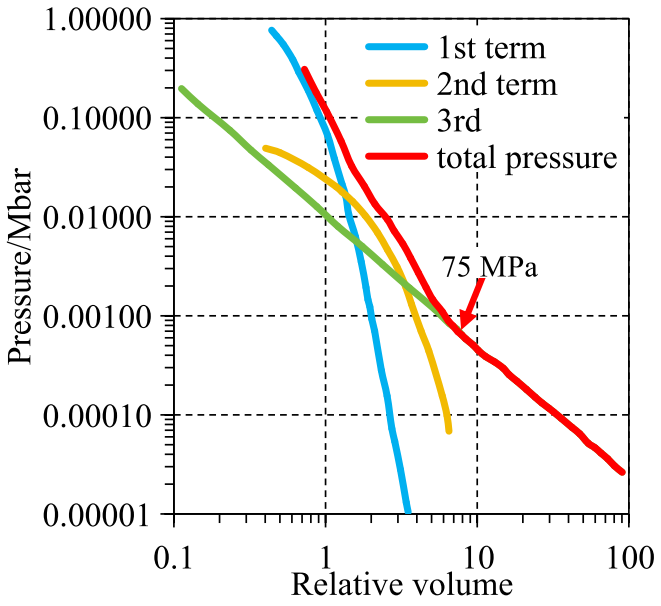

Fig. 3. Contribution of various terms in JWL equation of state to total adiabat pressure for Composition B, Grade A (Lee et al., 1968).

where E is the detonation energy per unit volume, its initial value is E_0. A, B, R_1, R_2, ω, are constants specific to the explosives. V is the dimensionless relative specific volume.

At any computational step, the pressure in an element with *MAT-HIGH_EXPLOSIVE_BURN is given by Equation (18) (LS-DYNA® Keyword User, 2021).

$$p = Fp_{\mathrm{eos}}(V, E) \qquad \text{Equation 18}$$

where p_{eos} is the pressure from the JWL equation; F denotes the burn fractions, and is given by max (F_1, F_2), where F_1 and F_2 are calculated by Equation (23) and Equation (24):

$$F_1 = \begin{cases} \dfrac{2(t - t_l)D_{\mathrm{CJ}}A_{e_{\max}}}{3v_e} & \text{if } t > t_l \\ 0 & \text{if } t \le t_l \end{cases} \qquad \text{Equation 19}$$

$$F_2 = \frac{1 - V}{1 - V_{CJ}} \qquad \text{Equation 20}$$

in which t_l is the lighting time and is computed for each fuel element by dividing the distance from the detonation point to the center of the element by the detonation velocity D_{CJ} in the initiation phase; $A_{e_{\max}}$ is the maximum projected area of an element; t is the current time; V_{CJ} is the C-J relative volume which equals to $1/\rho_{\mathrm{CJ}}$. If F surpasses 1, it is reset to 1.

3. Forecasting of C-J parameters

This section began by introducing the estimation of the detonable limit for a hydrogen-methane-air mixture, followed by the investigation delved into the effects of methane addition, fuel concentration, and initial temperature on detonation parameters. Finally, a predictive model is developed to forecast the C-J parameters which are essential for detonation modelling within hydrocode.

Given the primary focus of this study on deriving the C-J parameters for an H_2–CH_4-air mixture in detonation modelling, especially within the context of common industrial accidents, the initial pressure for the mixture was maintained at standard atmospheric pressure (101,325 Pa). The initial temperature varied from −20 °C to 40 °C, covering a wide spectrum of conditions encountered in daily life. In theoretical calculations, we assumed that the air consists of O_2 and N_2 with a volume ratio of 1:3.76 (Kao et al., 2023), neglecting other components constituting a small portion of the air.

Prior to theoretical calculations, it is imperative to estimate the detonable limit for a hydrogen-methane-air mixture. The detonable limit for hydrogen in air varies from 18.3 % to 59 % (V) (Biennial Report on Hydrogen Safety, 2007), and for methane-air mixtures, it falls between 5.3% and 15.6 % (vol) (Oran et al., 2015). This limit is influenced by varying ratios of hydrogen/methane in the air. If the concentration of the hydrogen-methane mixture exceeds the detonable limit, theoretical calculations may yield misleading detonation parameters. In this study, the methane percentage in the H_2–CH_4 mixture ranges from 0% to 100%. Unfortunately, there is a lack of data on the detonable limit when hydrogen is combined with methane. Determining the detonable limit for H_2–CH_4-air mixtures requires experimental work, which is beyond the scope of this study. Alternatively, the detonable limit for H_2–CH_4-air mixture was estimated using Le Chatelier's law (ABDELAAL et al., 2005), as expressed in Equation (21):

$$L_{\mathrm{m}} = \frac{100}{\sum_{i=1}^{n} \frac{V_i}{L_i}} \qquad \text{Equation 21}$$

where L_{m} represents the lower (upper) detonable limit of the fuel-air mixture, %; V_{i} denotes the volume ratio of the i-th combustible gas, %; L_{i} denotes the lower (upper) detonable limit of the i-th combustible gas, %. For instance, for a fuel composed of 90% hydrogen and 10% methane, its lower detonable limit LDL $= \frac{100}{90/18.3+10/5.3} = 14.7\%$, and the upper detonable limit UDL $= \frac{100}{90/59+10/15.6} = 46.2\%$. Le Chatelier's law is widely employed to determine the combustion limit for mixed fuels, and since the detonable process is a form of intense combustion, it is reasonable to use such a law to predict the detonable limit for H_2–CH_4-air mixtures.

3.1. The effect of methane addition

Fig. 4 depicts the effects of methane addition on C-J parameters, including detonation velocity, C-J pressure, heat capacity ratio, and detonation energy at stoichiometric fuel concentration. Given that methane is less reactive as compared to hydrogen, the detonation velocity exhibited a nonlinear decrease with increasing methane addition. For instance, at 20 °C, the detonation velocity decreased from 1970 m/s to 1804 m/s (an 8.4% reduction) as methane addition varied from 0 to 100%. The C-J pressure increased by 10.4% as the fuel varied from pure hydrogen to pure methane. The calculated detonation velocity and C-J pressure closely aligned with values in the literature (Bjerketvedt et al., 1997), with discrepancies of less than 0.1%. Additionally, consistent trends in detonation velocity and C-J pressure variations with methane addition were observed in experimental findings from reference (Bozier et al., 2009). The heat capacity ratio experienced slight changes at a constant initial temperature as methane increased, showing a marginal 0.4% increase when methane reached 100%. The detonation energy increased with the addition of methane, which can be attributed to that hydrogen possesses only about one-third of the combustion energy as compared to methane per unit volume (Chen et al., 2023b).

3.2. The effect of fuel concentration

Fig. 5 illustrates the influence of fuel concentration on the C-J parameters at 25 °C. The fuel concentration was characterized by the equivalence ratio of the fuel, $ER = \frac{\varphi_{\mathrm{fuel}}}{\varphi_{\mathrm{fuel-stoichiometric}}}$. The $\varphi_{\mathrm{fuel}} = \varphi_{\mathrm{CH_4}} + \varphi_{\mathrm{H_2}}$ is the total volume ratio of fuel (H_2 and CH_4) in air, and the $\varphi_{\mathrm{fuel-stoichiometric}}$ represents the volume fuel ratio in air when the corresponding percentage of fuel is totally consumed, with neither fuel nor oxygen left after the reaction. An ER of 1 implies that the oxygen in the air is precisely sufficient to react with the fuel, while an ER less than 1

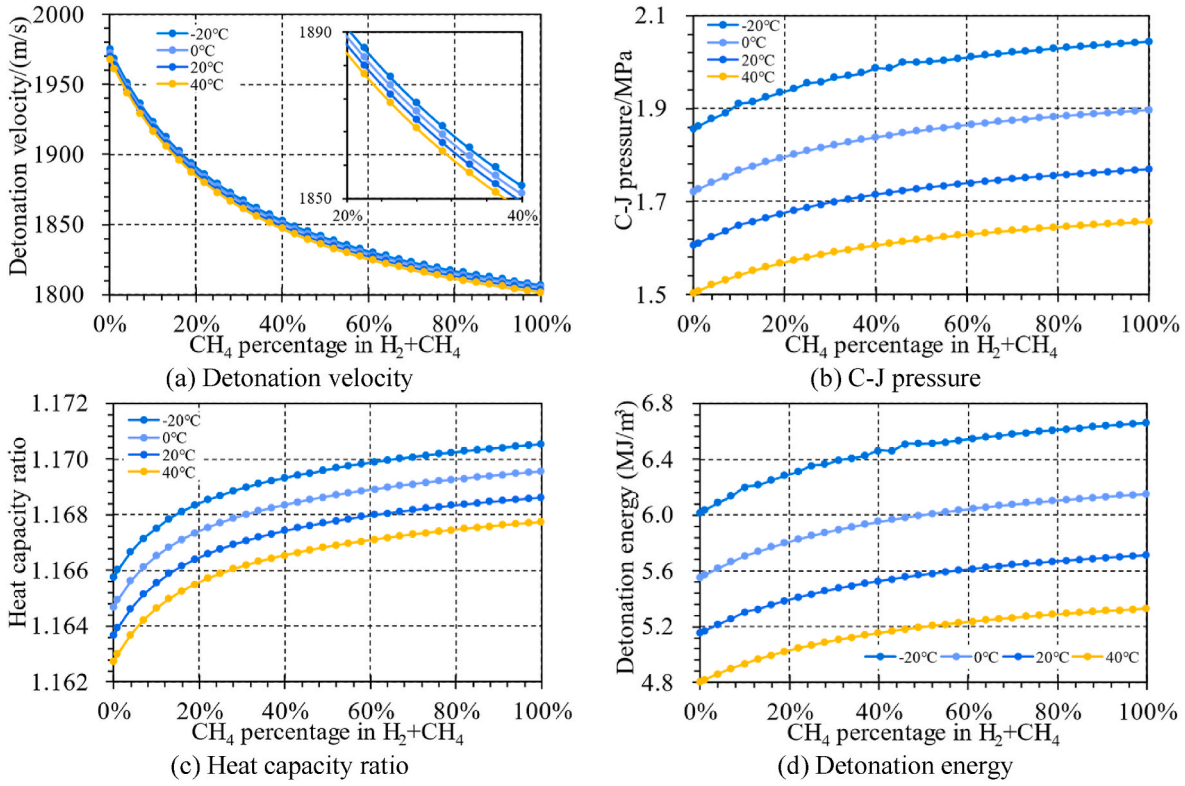

Fig. 4. Influence of methane addition on C-J parameters, the fuel concentration is at stoichiometric ($ER = 1$).

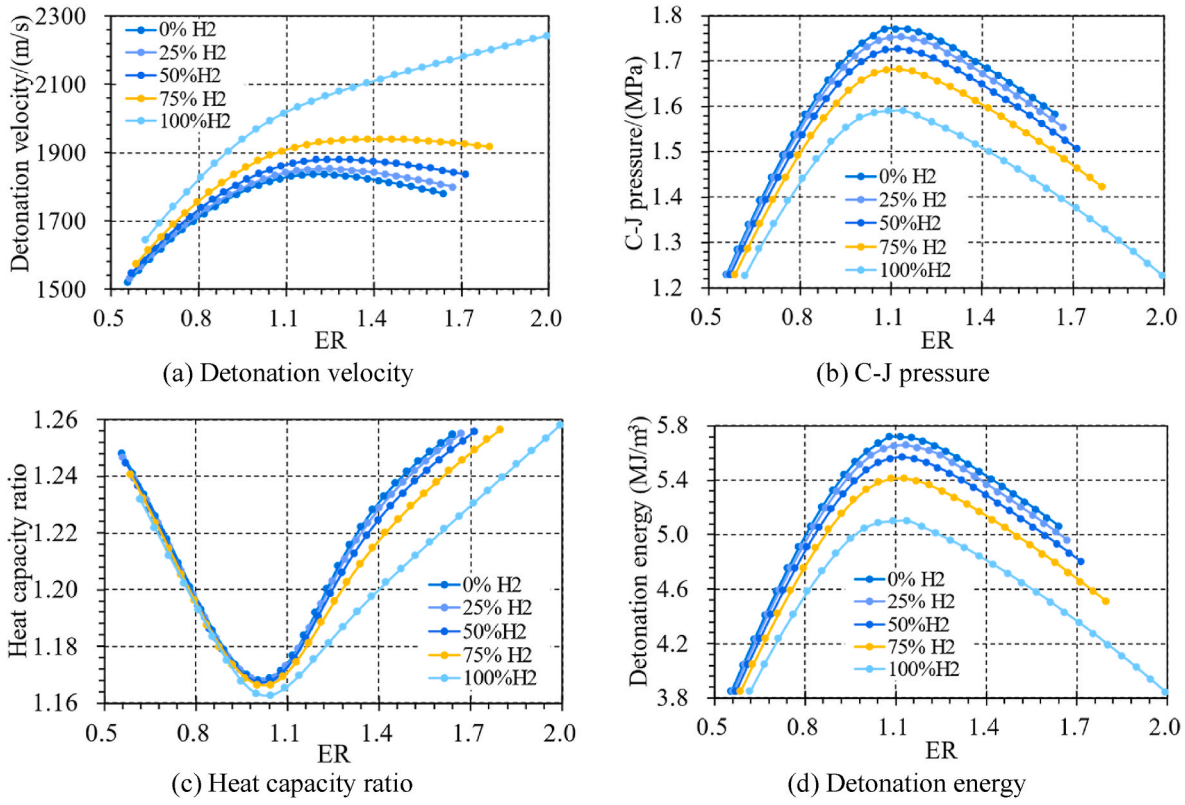

Fig. 5. Influence of fuel concentration on C-J parameters, and $ER = 1$ represents fuel is totally consumed, with neither fuel nor oxygen left after reaction.

indicates an excess of oxygen, defining a lean fuel mixture. Conversely, an ER greater than 1 characterizes a rich fuel mixture.

As shown in Fig. 5, the inclusion of methane narrows the detonable range of hydrogen while extending the lower detonable limit. As ER increased, the detonation velocity experienced a continuous ascent from 1644 m/s to 2242 m/s (a 36.4% increase) as the fuel concentration

varied from the lower detonable limit to the upper detonable limit for pure hydrogen. By comparison, for hydrogen-methane-air mixtures, the detonation velocity showed an initial increase until the ER slightly exceeded 1, after which it began to decrease with further increments of ER. The C-J pressure reached its peak as ER was near 1.1 and demonstrated a declining trend as the ER expanded towards lower or upper detonation limit. This observed trend aligns with experimental findings in reference (Bozier et al., 2009). The detonation energy also attained its peak value around an ER of 1.1. However, the heat capacity ratio had its lowest value (dropped by 7.4% as compared to its highest value) as the fuel concentration was near stoichiometric and increased as ER deviated away from approximately 1.1. This phenomenon can be attributed to the highest detonation temperature at C-J conditions when the fuel concentration is near stoichiometric. For example, the calculation result showed that, for pure hydrogen at an initial temperature of 25 °C, the detonation temperature was 2975 °C when *ER* was 1.1, decreasing to 2275 °C and 2242 °C as the fuel concentration reaches the lower (18.3%) and upper (59%) detonable limits, respectively. The heat capacity ratio decreases as the gas temperature increases (White, 1990).

3.3. The effect of initial temperature

The rising initial temperature had a negative effect on C-J parameters, as shown in Fig. 6. In particular, the initial temperature exerted minor influence on detonation velocity and heat capacity ratio. For instance, in the case of pure hydrogen, their values only decreased by 0.3% and 0.2%, respectively, as the initial temperature increased from −20 °C to 40 °C. In contrast, the initial temperature had a notable impact on C-J pressure and detonation energy, showcasing an almost linear downward trend with increasing initial temperature. This negative relationship contradicts the fact that unburned gas tends to exhibit higher chemical reactivity as the initial temperature increases. However, a similar negative trend in detonation velocity and pressure concerning initial temperature was observed in experiments in literature (Edwards et al., 1959; Kuznetsov et al., 2022), in which such a negative trend was attributed to the higher density and viscosity at lower initial temperatures.

3.4. Predicting models for C-J parameters

Utilizing the ideal gas assumption, the initial density (ρ) of an H_2–CH_4-air mixture at standard atmospheric pressure (101,325 Pa) is solely dependent on the temperature (T) and the percentages of hydrogen (Φ_{H2}) and methane (Φ_{CH4}) in the H_2–CH_4-air mixture. This relationship can be expressed by Equation (22):

$$\rho = \frac{298.15}{T}\left[0.0824\varphi_{H_2} + 0.6557\varphi_{CH_4} + 1.1793\left(1 - \varphi_{H_2} - \varphi_{CH_4}\right)\right] \quad \text{Equation 22}$$

where ρ represents the density of H_2–CH_4-air mixture, kg/m^3.

A generalized formula predicting other critical C-J parameters, including detonation velocity (D_{CJ}), C-J pressure (P_{CJ}), heat capacity ratio at C-J condition (γ_{CJ}), detonation energy per unit volume ($Q_{CJ\text{-}V}$), and detonation energy per unit mass ($Q_{CJ\text{-}M}$), crucial for hydrocode simulations of detonation phenomena, was derived using a power formula incorporating initial temperature (T), and two quadratic polynomials related to the ratio of methane (C_{CH_4}) and the equivalence ratio of the fuel (ER) and was expressed by Equation (23) to Equation (25).

$$\left(D_{CJ}, P_{CJ}, \gamma_{CJ}, Q_{CJ-V}, Q_{CJ-M}\right) = A_0\left(\frac{298.15}{T}\right)^{a_1} \cdot f\left(C_{CH_4}\right) \cdot f(ER) \quad \text{Equation 23}$$

$$f\left(C_{CH_4}\right) = \left(a_2 + a_3 C_{CH_4} + a_4 C_{CH_4}^2 + a_5 C_{CH_4}^3 + a_6 C_{CH_4}^4\right) \quad \text{Equation 24}$$

$$f(ER) = \left(a_7 + a_8 ER + a_9 ER^2 + a_{10} ER^3 + a_{11} ER^4\right) \quad \text{Equation 25}$$

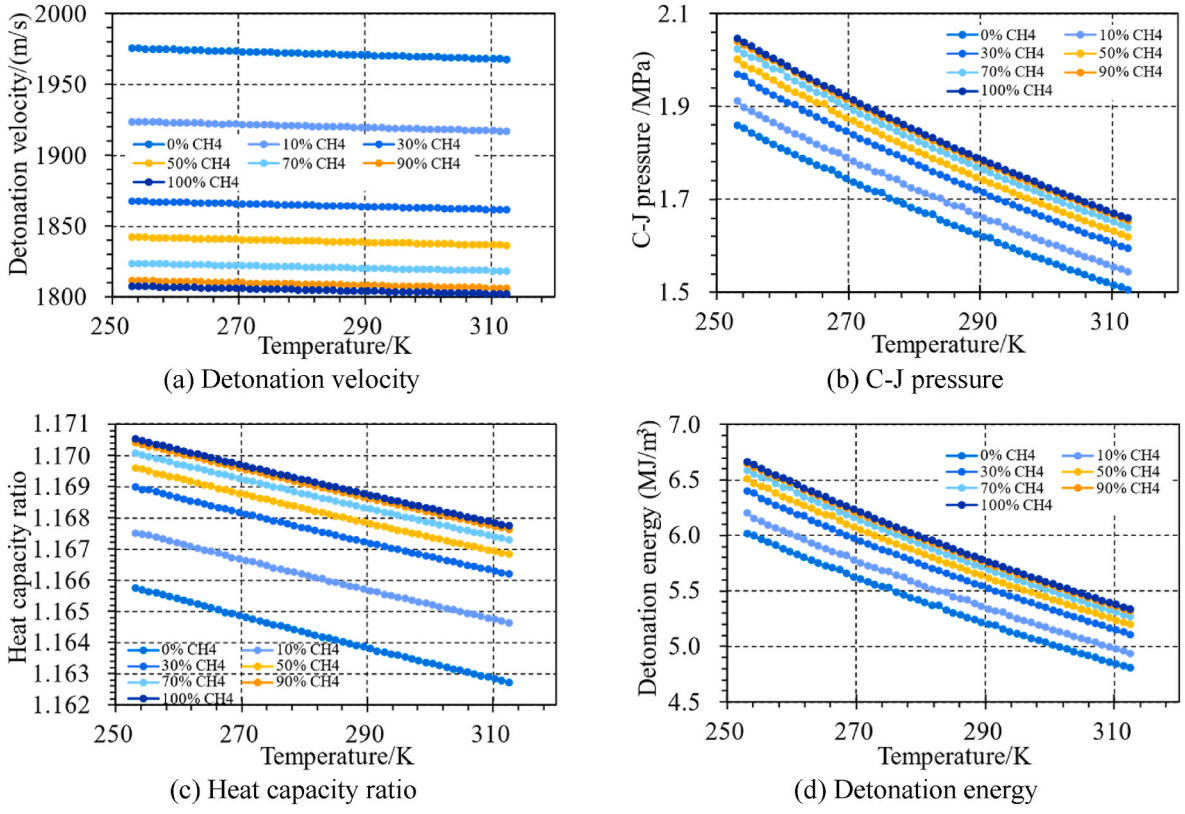

Fig. 6. Influence of initial temperature on C-J parameters, the fuel concentration is at stoichiometric (ER = 1).

where A_0 denotes the C-J parameters (D_{CJ}, P_{CJ}, γ_{CJ}, $Q_{CJ\text{-}V}$, $Q_{CJ\text{-}M}$) at 25 °C initial temperature and 29.5%(V) H_2-air mixture; a_1 to a_{11} are the fitting coefficients; D_{CJ} denotes the detonation velocity, m/s; P_{CJ} is the C-J pressure, MPa; γ_{CJ} represents the heat capacity ratio prediction in C-J condition; $Q_{CJ\text{-}V}$ is the detonation energy per unit volume, MJ/m^3; $Q_{CJ\text{-}M}$ is the detonation energy per unit mass, MJ/kg; T denotes the initial temperature, K; $C_{CH_4} = \frac{\varphi_{CH_4}}{\varphi_{H_2}+\varphi_{CH_4}}$ is the volume ratio of methane in the hydrogen-methane fuel, and Φ_{H2} and Φ_{CH4} represent the volume ratios of hydrogen and methane in the H_2–CH_4-air mixture, respectively.

The coefficients in Equation (23) to Equation (25) were determined using the least squares method based on the theoretical calculation results, and their values are shown in Table 2. As initial temperature had negligible effect on detonation velocity and heat capacity ratio, a_1 for them was set as 0. $a_1 = 1$ for C-J pressure and detonation energy per unit volume as linear relation with initial temperature was observed before. For H_2-air mixture at 25 °C and 29.5% (V) concentration (representing room conditions with the severest concentration), its C-J parameters are the same as A_0. The goodness of fitting (R^2) is between 0.95 and 0.99, indicating that the equations for predicting C-J parameters have high accuracy.

4. Validation of the modelling approach

To validate the proposed modelling approach, a comparative analysis was conducted between numerical results and experimental data gathered from seven distinct scenarios (Machniewski et al., 2022; GROETHE et al., 2007; Rehm et al., 1993; Nozu et al., 2005; Mueschke et al., 2020; Zbikowski et al., 2010; Zipf et al., 2013; Gamezo et al., 2012; Porowski et al., 2013). These experiments covered a diverse range of conditions, spanning industrial-scale setups (excluding the last group) involving H_2-air, CH_4-air, and H_2–CH_4-air mixtures. The tests explored concentrations from near the lower detonable limit to the upper detonable limit, varying in scale from small dimensions (0.14 m diameter with 6 m length) to large-scale configurations (300 m^3). The experiments were carried out in various environments, including open-air fields, open-air fields with blast walls, semiconfined fields, and totally confined fields. Geometric shapes ranged from simple forms like hemispherical, cubic, and cylindrical to highly complex geometries featuring channels and canyons in a tunnel. An overview of experimental tests is illustrated in Table 3.

Utilizing the predicted C-J parameters, the LS-DYNA hydrocode was employed to model the detonation and blast propagation processes in the conducted experiments. The multi-material arbitrary Lagrangian Eulerian (MMALE) approach was utilized to model the flow field and the interaction between structural response and dynamic loading (Souli et al., 2004). As mentioned before, The *MAT-HIGH_EXPLOSIVE_BURN material model in combine with the *EOS_JWL equation of state model, was chosen to model the gas-air mixture. The state of ambient air in the study was described using *MAT_NULL and *EOS_LINEAR_POLYNOMIAL, and the corresponding parameters can be referenced in (Chen et al., 2023b). Part of the relevant keywords in the current study has been made open source and is accessible on the website (Chen, 2023).

Table 3
Overview of the experimental tests for the validation of C-J parameters in hydrocode (Machniewski et al., 2022; GROETHE et al., 2007; Rehm et al., 1993; Nozu et al., 2005; Mueschke et al., 2020; Zbikowski et al., 2010; Zipf et al., 2013; Gamezo et al., 2012; Porowski et al., 2013).

NO.	Fuel	Concentration	Geometry	Comments
1	H_2	18.52%,19.07%, 20.0%, 20.5%, 26.91%, 29.05%	≈50 m^3, hemispherical, free air	6 tests, from lower detonable limit to stoichiometric concentration
2	H_2	30%	300 m^3, hemispherical, free air	1 test, stoichiometric concentration
3	H_2	29.5%	5.27 m^3, cubic, free air with blast wall	1 test, stoichiometric concentration
4	H_2	29.5%	0.283 m^3, cubic, semi-confined	1 tests, stoichiometric concentration
5	H_2	20%, 25.5%	263 m^3, irregular, totally-confined tunnel	2 tests, lower detonable limit to near stoichiometric concentration
6	CH_4	5.3%, 7.3%, 10.2%, 14%	63.4 m3, cylindrical, semi-confined, one end closed, one open to air	4 tests, from lower to near upper detonable limit
7	CH_4–H_2	0%–50% CH_4 in H_2–CH_4	0.14 m diameter, 6 m long, cylindrical, both end closed	Stoichiometric concentration, 10% CH_4 for comparison

Note: (1) The volume mentioned above refers to the size of the fuel-air mixture. (2) In the last group, the concentration represents the percentage of CH_4 in the CH_4–H_2 mixture, and the overall fuel concentration is stoichiometric.

4.1. Hydrogen-air detonation

This section presented the modelling of hydrogen-air detonation, where the results were from the largest scale experiments available in open literature.

4.1.1. 50 m^3 hemispherical hydrogen-air detonation

Six series of H_2-air detonation tests were carried out in open-air space (Rehm et al., 1993), with the corresponding conditions outlined in Table 4. The homogeneous H_2-air mixture was enclosed in a hemispheric polyethylene film with volume of approximately 50 m^3, and a diameter

Table 2
Coefficients for predicting C-J parameters.

Parameters	A_0	a_1	a_2	a_3	a_4	a_5	a_6
D_{CJ}	1969	0	1.22864	−0.57647	1.09676	−1.02206	0.35897
P_{CJ}	1.576	1	0.61741	0.21478	−0.34747	0.31390	−0.11270
γ_{CJ}	1.163	0	0.36429	0.01326	−0.01400	0.00208	0.00280
$Q_{CJ\text{-}V}$	5.388	1	0.68023	0.17976	−0.31156	0.31322	−0.12413
$Q_{CJ\text{-}M}$	3.499	0.03321	2.97402	−3.10004	6.10571	−5.83608	2.09381
Parameters	a_7	a_8	a_9	a_{10}	a_{11}	R^2	–
D_{CJ}	0.69548	−0.64173	1.82362	−1.36499	0.32177	0.96	–
P_{CJ}	−0.44207	3.86728	−1.85023	−0.13801	0.15668	0.99	–
γ_{CJ}	3.71461	−1.93343	0.82571	0.33006	−0.17904	0.95	–
$Q_{CJ\text{-}V}$	−0.69056	3.45302	−0.50147	−1.22255	0.41354	0.99	–
$Q_{CJ\text{-}M}$	0.23459	−0.71115	1.92235	−1.42178	0.32880	0.96	

Note: The fitting was based on theoretical calculation results under the initial conditions of 101,325 Pa, −20 to 40 °C, and within the detonable limit of H_2–CH_4-air mixture, where either H_2 or CH_4 can be zero.

Table 4
Experiment condition of the six tests.

Test	Volume (m^3)	Temperature (K)	Concentration (vol%)	Radius (m)	Remarks
1	53	304	29.05	2.94	Stable detonation
2	50	301	18.52	2.88	Unstable detonation
3	50	308	26.91	2.88	Stable detonation
4	50.2	295	19.07	2.88	Unstable detonation
5	51.1	298	20.5	2.90	Unstable detonation
6	51	298	20.0	2.90	Unstable detonation

of about 2.9 m. The hydrogen concentration ranged from 18.53% (near lower detonable limit of 18.3%) to 29.05% (close to stoichiometric concentration of 29.5%).

The detonation was initiated by a 50 g high explosive at the bottom center of the hemisphere. Overpressure data were recorded by 11 pressure gauges positioned inside and outside of the hemisphere, mounted on the surface. The experimental setups are depicted in Fig. 7. For tests 1 to 4, the gauges were located between 0.75 m and 10 m away from the ignition point. By comparison, for tests 5 and 6, six gauges were placed inside the hemisphere, with a distance of 2.75 m, while the other five were located 3.25 m away from the ignition point, outside of the fuel.

The scenario was simplified as a 1-D problem with 1 mm mesh, and the polyethylene film was neglected. The C-J parameters used for the detonation simulation are shown in Table 5.

The simulation results for Test 1 (near stoichiometric concentration) and Test 5 (near lower detonable limit concentration) are presented in Fig. 8. Both the pressure peak and variation trend matched well with the experimental data when the hydrogen concentration was 29.05%. However, when the hydrogen concentration decreased to 20.5%, which was near the lower detonable limit, the detonation became unstable, as evidenced by the notable oscillation of the pressure history. As shown in Fig. 8 (b), at the distance of 2.75 m, the numerical results matched the experimental data with reasonable accuracy as compared to gauges 1 to 4. However, for gauges 5 and 6, the pressure dropped from about 2 MPa to near 0.3 MPa even with the same distance. At the distance of 3.25 m, the numerical prediction kept a similar trend in comparison with the experiment results but slightly overestimated the peak pressure. Since the numerical model was based on the stable detonation assumption, so it was not surprising to observe this discrepancy when the detonation was unstable. Fortunately, the numerical model provided conservative prediction when the detonation becomes unstable, which is beneficial for safe engineering design.

4.1.2. 300 m^3 hemispherical hydrogen-air detonation

Another larger-scale H_2-air detonation test with 30% (V) concentration and a 300 m^3 volume was conducted in open-air space (GROETHE et al., 2007). The fuel, covered in plastic film with a height of 5.7 m, deviated from an ideal hemisphere. However, as shown in Fig. 9, the shape of the fuel was simplified as hemispherical with a radius of 5.2 m. The detonation was initiated by a 10 g C4 high explosive at the bottom of the mixture. Pressure gauges were placed on the surface from 4.1 m (inside the fuel) to 15.61 m. The scenario was modeled in 1D with 1 mm mesh. Assume the initial temperature was 20 °C, and the C-J parameters for the 30% H_2-air mixture are presented in Table 5.

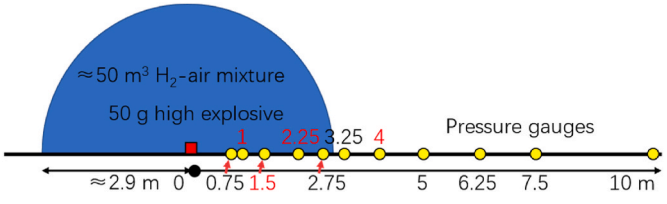

Fig. 7. Experimental setups for the 50 m^3 H_2-air detonation test in open-air space (test 1 to 4; for test 5 and 6, six gauges located 2.75 m away from the ignition point, while another six were 3.25 m away) (Rehm et al., 1993).

Fig. 10 displays the load comparison between numerical and experimental results. The difference in peak pressure between numerical and experimental results ranged from −4% to 45%, which can be considered reasonable accuracy due to potential uncertainties in such a large-scale test. The reference (GROETHE et al., 2007) only provided the pressure history at 15.61 m, as illustrated in Fig. 10 (b). It can be observed that the numerical model accurately captured the pressure peak, pressure trend and impulse with deviations of 14% and 6%, respectively.

4.1.3. Hydrogen detonation with blast wall

This section examined the performance of the developed numerical model in an open-air space with a blast wall (Nozu et al., 2005). As depicted in Fig. 11, a cuboid 30% (V) H_2-air mixture with a volume of 5.27 m^3 stood at 4 m away from a reinforced concrete wall. The concrete wall, measuring 10 m in length, 2 m in height and 0.15 m in thickness, was modeled as rigid due to its minimal displacement in the experiment (a few millimeters). A 10 g C4 high explosive was placed at the bottom center of the fuel mixture to initiate direct detonation. Pressure gauges were placed in front of the wall, on the wall and after the wall to trace pressure development.

A 3D numerical model was employed to simulate this test with a mesh of 2.5 cm in the core region, and only half of the scenario was established due to its symmetric nature. The mesh was stretched to the boundary to avoid boundary effects. The size of the model was 11 m × 16 m × 11 m (L × W × H), and the total number of mesh was about 13 million. This case utilized the identical C-J parameters presented in in Table 5.

Figs. 12 and 13 illustrate the peak pressure and load history comparison. Once again, the main trend of blast development was successfully captured by the proposed model, providing reasonable accuracy in terms of peak pressure, pressure history, and impulse.

4.1.4. Hydrogen detonation in semi-confined space

A 30% (V) hydorgen explosion test inside a steel chamber (Mueschke et al., 2020) was utilized to assess the performance of the proposed model in semi-confined space. As illustrated in Fig. 14, the steel chamber had internal dimensions of about 1.8 m × 1.8 m × 1.8 m, with the front face of the chamber open to air, and a partial wall extended from the ceiling of chanmber with a length of 0.61 m. The fuel mixture was placed at the bottom center of the chamebr, and was initiared by a 6 g C4 high explosive. As the scenario was symmetrical, only half of scenario was modeled. The pressure sensors were installed inside the chamber wall, and the fuel mixtue, containing in a plastic bag with a volume of 0.283 m^3, was simplified as a cuboid with a size of 1.12m × 1.12m × 0.23. The mesh size inside the chamber was 6.25 mm, and was expanded enough to the boundary to avoid boundary effect. The total mesh number was approximately 16 million. This case utilized the identical C-J parameters are presented in Table 5.

The load history comparison is displayed in Fig. 15. Owing to the complexity of the geometry, the load exhbited a much more intricate shape, and multiple pressure peaks were observed due to the multiple reflections inside the chamber. Despite this complexity, the numerical model still accurately captured the pressure peaks and variation trend on the righ wall, left wall and ceiling of the chamber. Furthermore, the reflected waves were predicted to some extent of precision.

The proposed model's accuracy and efficiency were compared with the detailed chemistry approach implemented in LS-DYNA using the CESE compressible CFD solver and a structural FEM solver (Chen et al.,

Table 5
Detonation properties for the H_2-air mixture, unit system is kg-m-s, $\omega = \gamma_{CJ}$-1.

Mixture	Density	Detonation velocity	P_{CJ}	ω	E_0	Comments
29.05% H_2-air	0.84	1957	1.54×10^6	0.164	5.23×10^6	Secction 4.1.1
20.5% H_2-air	0.95	1720	1.32×10^6	0.216	4.16×10^6	
30% H_2-air	0.87	1970	1.60×10^6	0.160	5.49×10^6	Section 4.1.2, 4.1.3, 4.1.4
20% H_2-air	0.98	1703	1.32×10^6	0.219	4.14×10^6	Section 4.1.5
25.5% H_2-air	0.91	1872	1.51×10^6	0.182	5.06×10^6	
5.3% CH_4-air	1.15	1521	1.23×10^6	0.248	3.64×10^6	Section 4.2
7.3% CH_4-air	1.14	1690	1.52×10^6	0.204	4.90×10^6	
10.2% CH_4-air	1.13	1822	1.77×10^6	0.171	5.92×10^6	
14.0% CH_4-air	1.11	1810	1.66×10^6	0.240	5.28×10^6	
33.3% CH_4–O_2	1.09	2391	2.97×10^6	0.131	11.86×10^6	

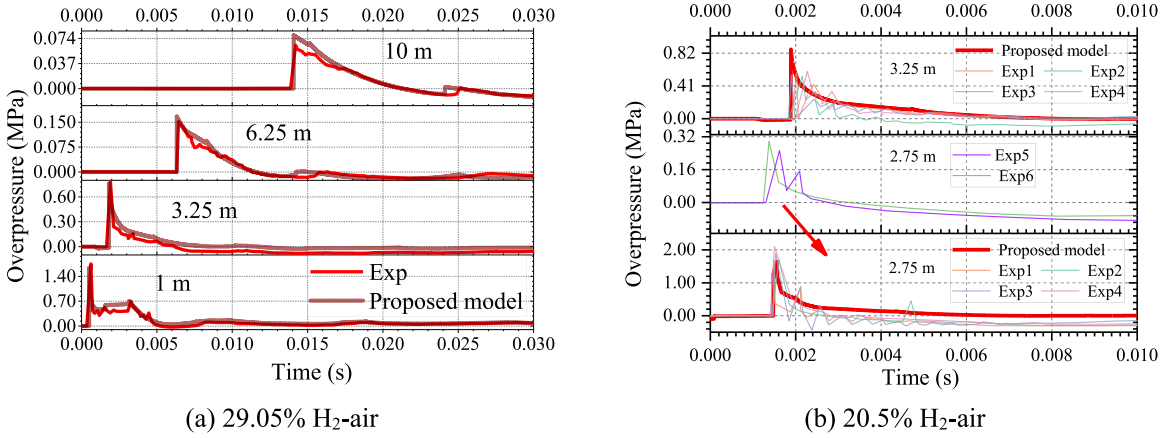

(a) 29.05% H_2-air (b) 20.5% H_2-air

Fig. 8. Pressure history comparison (Rehm et al., 1993).

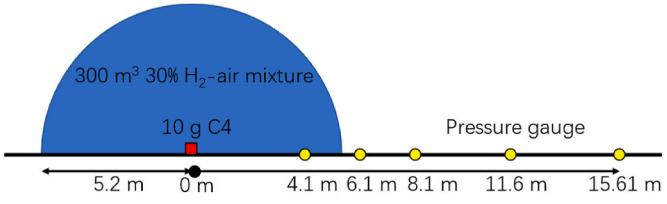

Fig. 9. Experimental setups for the 300 m^3 30% H_2-air detonation test in open-air space (GROETHE et al., 2007).

2023b). Both methods utilized the same mesh size and boundary conditions on a high-performance computer with 28 CPU cores. While the load magnitude and variation trends were comparable, the CESE coupling method suffered from pressure smearing due to insufficient mesh resolution (6.25 mm) for capturing the detonation structure with detailed chemistry, leading to a slower pressure rise. The proposed model, by avoiding the simulation of expensive detailed chemical reactions, achieved a significant 90% reduction in computational time in contrast with the CESE method (9.6 h vs. 124.3 h).

4.1.5. *RTU large scale confined complex geometry*

Benchmark experimental results from the RTU facility for the Hysafe project, founded by European Union (Zbikowski et al., 2010), were utilized to examine the capability of the proposed model. As shown in Fig. 16 and Table 6, the tests were conducted in a fully confined tunnel with a complex geometric shape, consisting of a reinforced concrete structure lined with steel. The tunnel dimensions (maximum) were 27.55 m in length, 6.3 m in depth, and 6.55 m in width, resulting in a volume of 263 m^3. Fig. 16 illustrates the tunnel's vertex coordinates, ignition point locations, and pressure gauge positions (Yáñez et al., 2011b). This study utilized data from two tests, namely HYD05 and

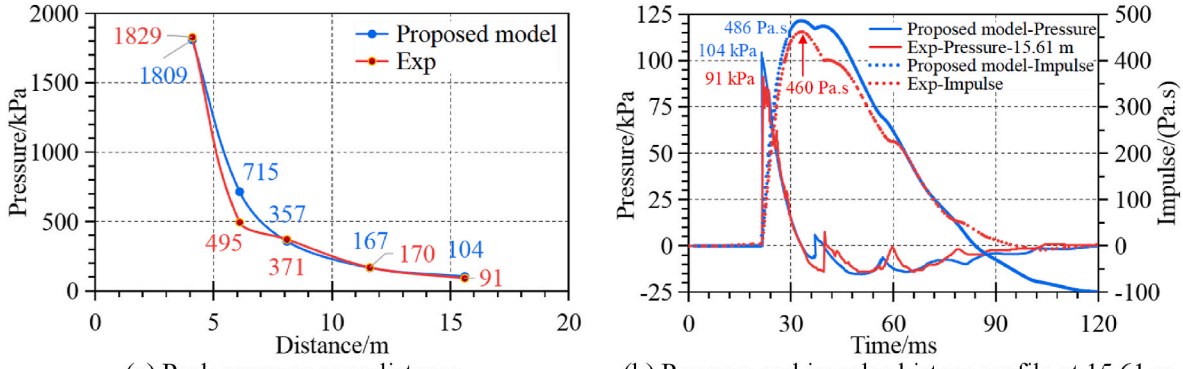

(a) Peak pressure over distance (b) Pressure and impulse history profile at 15.61 m

Fig. 10. Load comparison between numerical and experimental results (GROETHE et al., 2007).

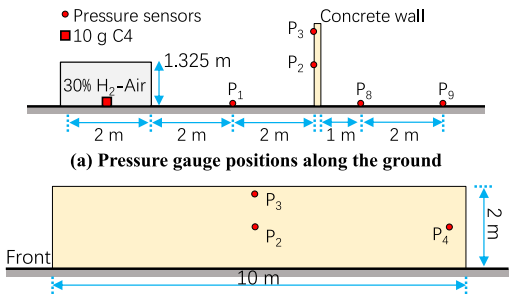

Fig. 11. The distribution of pressure sensors (Nozu et al., 2005).

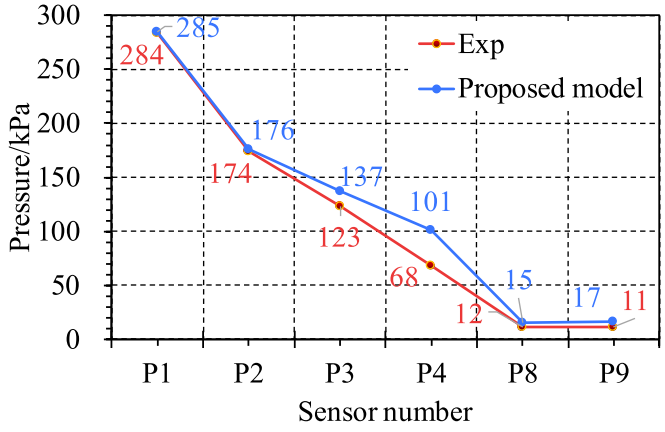

Fig. 12. Pressure peak comparison between numerical and experimental results (Nozu et al., 2005).

HYD09, with uniform hydrogen-air mixtures containing concentrations of 20% and 25.5%, respectively. The detonations were initiated by a 200 g high explosive, with initial conditions set at 20 °C and 1 atm pressure (Yáñez et al., 2011b). Pressure gauges 2 to 5 were mounted on the front wall, gauges 1 and 6 were positioned at the middle of the transversal wall, and gauges 7 to 12 were affixed to the rear wall of the tunnel. The data from gauges 2 to 5 in HYD05 and gauges 7 to 11 in HYD09 were publicly available. A 3D numerical model was established with a mesh resolution of 5 cm, totaling approximately 2.3 million mesh elements. The C-J parameters used are detailed in Table 5.

Because of the reliability of the RTU test results, other numerical models (Machniewski et al., 2022; Zhang et al., 2019), incorporating chemical reactions, also compared their outcomes with the RTU results. It should be noted that, unlike the hydrogen code such as LS-DYNA, previous numerical models were based on pure CFD codes, which have limited capabilities in addressing structural responses with high strain rate effects and large deformation scenarios. This is the first time such experiments were modeled in a hydrocode.

The load history comparison from numerical, experimental and reference (Machniewski et al., 2022; Zhang et al., 2019) results, is shown in Fig. 17. It can be observed that, with the similar spatial resolution, the proposed model outperformed the current practice of numerical simulation, providing better peak pressure prediction and pressure variation trend projection. For example, the pressure history shown in Fig. 17 (a) was based on a one-step chemical reaction model (Zhang et al., 2019), which gave a much lower peak pressure prediction (underestimated by a half), and the latter reflection waves was almost not captured at all. Both LS-DYNA and the study in reference (Zhang et al., 2019) underestimated the peak pressure at P_5 significantly, potentially because P_5 is very close to the 200 g high explosive initiator. Therefore, the pressure captured by P_5 can be significantly affected by the initiator. Also, such a strong detonator may cause over-driven detonation, which has a much higher detonation pressure. However, the influence of the initiator and over-driven effect was hard to model in the numerical model. Despite the limitation, LS-DYNA also gave a better peak pressure prediction with a value of 2.43 MPa, as compared to the result of 1.51 MPa from reference (Zhang et al., 2019). Another numerical results, shown in Fig. 17 (b), which also used the same mesh size of 5 cm (Machniewski et al., 2022), was based on the mature CFD code, Fluent, incorporating with a one-step chemical reaction, tending to provide lower predictions compared to the proposed model.

Several factors contributed to the discrepancies between the

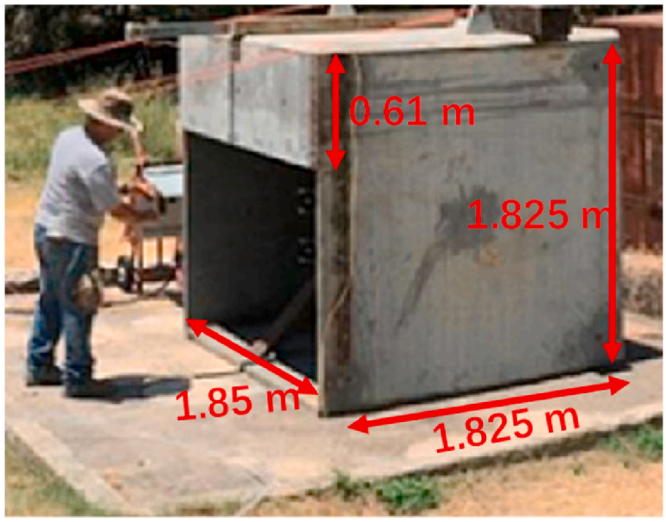

Fig. 14. Site image of the experiment (Mueschke et al., 2020).

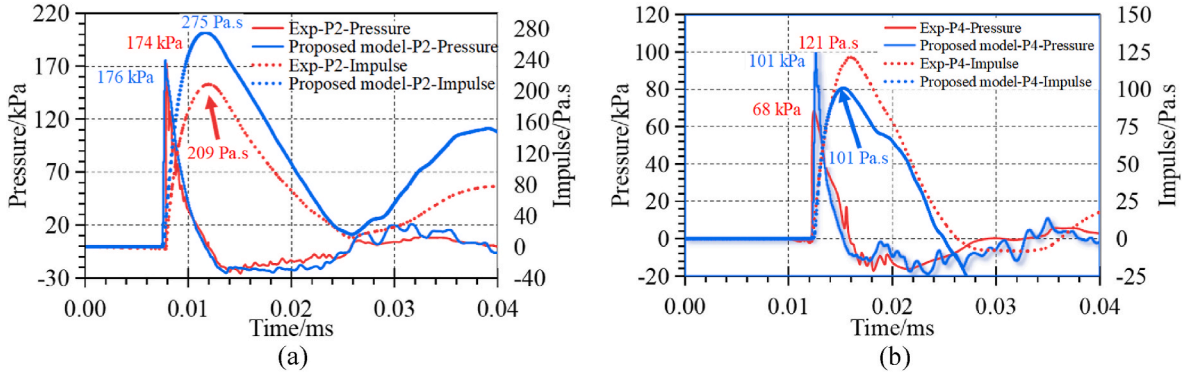

Fig. 13. Load history comparison between numerical and experimental results (Nozu et al., 2005).

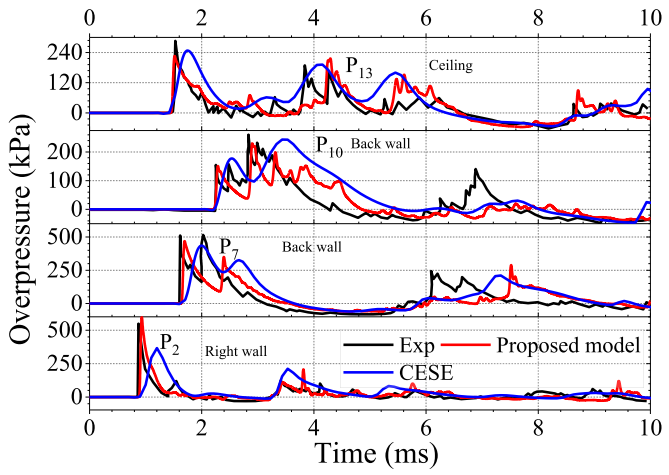

Fig. 15. Load history comparison between numerical and experimental results (Mueschke et al., 2020).

proposed model and previous models incorporating chemical reactions during CFD simulation. Notably, previous studies suggest that accurate reproduction of the gas detonation process requires solving the internal 3D structure of the detonation wave, necessitating a spatial resolution at least one order of magnitude smaller than the detonation cell size (e.g., below 1 mm for a 30% H_2-air mixture) (Bozier et al., 2009; GROETHE et al., 2007). However, models in references (Machniewski et al., 2022; Zhang et al., 2019) employed coarser mesh sizes due to computational limitations. Conversely, the proposed model utilizes external tools to handle the energy release process, eliminating the need for an extremely fine mesh to capture the detonation structures. This remarkably reduces computational demands while achieving higher accuracy, offering a compelling alternative for modelling gas detonation processes that balances fidelity and efficiency.

4.2. Methane-air detonation

Limited experimental data are available for methane-air detonation, primarily because methane-air is considered the least sensitive hydrocarbon-air mixture regarding detonation initiation (Gamezo et al., 2012). This is attributed to the inherent stability of methane molecules, rendering it challenging to induce detonation reactions. Till now, there is still no confirmed report about successful self-supported detonation in unconfined methane-air mixtures. This section provided the modelling of methane-air detonation which had the largest scale in publicly available data. As shown in Fig. 18, a series of CH_4-air detonation tests were carried out in a steel tube with dimensions of 73.2 m long and 105 cm internal diameter (Zipf et al., 2013; Gamezo et al., 2012). One side of

Table 6
Experiment condition of the two tests (Zbikowski et al., 2010).

Exp ID	H_2 % (vol)	T	P	Ignition location	Gagues
HYD05	20%	20 °C	1 atm	At the corner of the canyon, 0.8 m above the floor and 0.5 m from the wall	2 to 5 mounted on the front wall of the canyon, 1 and 6 are located at the middle of transversal wall
HYD09	25.5%			At the end of the curved channel, 0.8 m above the floor and 0.5 m from the wall	7 to 12 mounted on the rear wall of the channnel

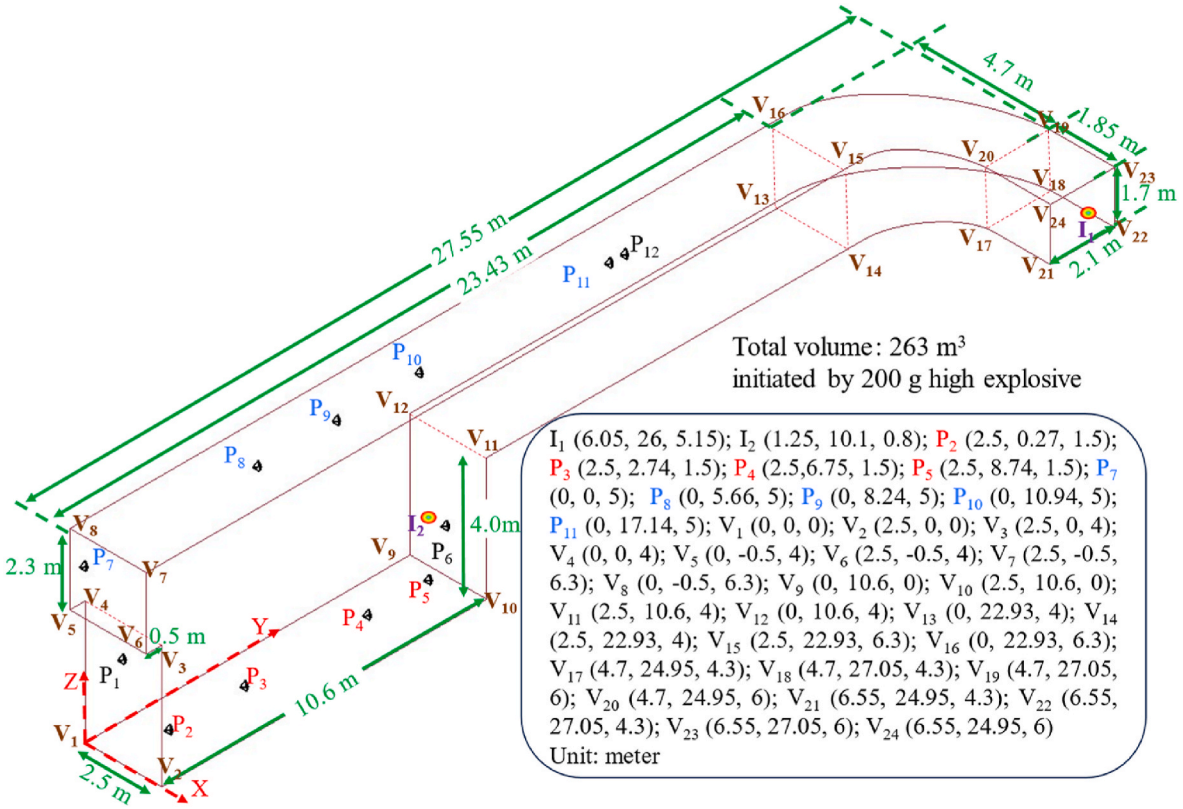

Fig. 16. Experimental facility scheme: I_1 and I_2 are the ignition point for 25.5% and 20% H_2-air detonation, respectively; P_2 to P_5 are mounted on the front wall; P_7 to P_{12} are mounted on the back wall; P_1 and P_6 are located at the middle of transversal wall; V_1 to V_{24} represent vertex of the tunnel; the coordinates of the aforementioned points are provided in the lower right box; the sections V_{13}–V_{16} and V_{17}–V_{20} are assumed to be arc transitions (Zbikowski et al., 2010; Zhang et al., 2019).

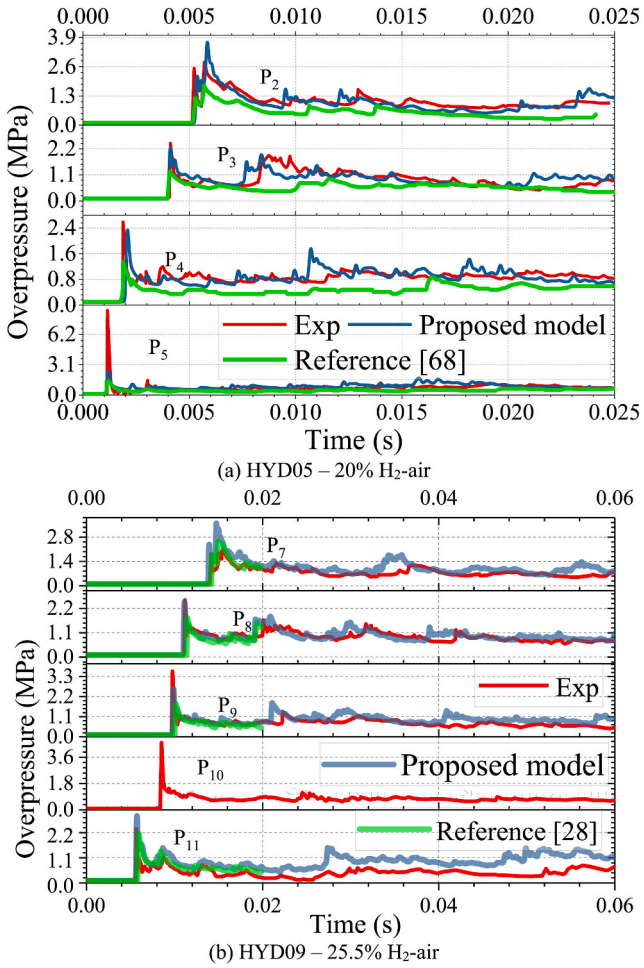

Fig. 17. Load history comparison among numerical, experimental results and reference (Machniewski et al., 2022; Yáñez et al., 2011b; Zhang et al., 2019).

the tube is closed, while the other side is open to air. The detonation was initiated by a stoichiometric CH_4–O_2 bag with a length of about 3.7 m. The CH_4–O_2 bag was ignited at 0.5 m away from the closed end. The rest of the tube was filled with homogeneous CH_4-air mixture. The publicly accessible results were from a CH_4-air concentration of 5.3%–14% (V), which almost covered the methane-air detonation range (5.3%–15.6). Pressure gauges were mounted on the internal wall of the tube, and the initial condition was assumed to be 25 °C and 1 atm. Respectively.

The scenario was represented by a 2D symmetric model with a 5 mm mesh resolution, and the total mesh magnitude was about 2.9 million. The CH_4–O_2 mixture was also considered in the numerical model, and the C-J parameters used for the modelling are depicted in Table 5.

The load history comparison is presented in Fig. 19. It can be observed that the proposed model predicted the pressure history with descent accuracy when the methane concentration was distant from the detonation limit. The magnitude of the pressure peak closely matched the experimental data, although the numerical model exhibited a slower decay trend. This deceleration can be attributed to the neglect of heat transfer with the environment in the numerical model. While the predicted pressure peaks were understandably lower than the experimental ones owing to the stable C-J detonation assumption of the proposed model, it is important to acknowledge that the real detonation structure is a 3D zone consisting of multiple detonation cells. In this complex structure, the pressure inside the detonation cell is uneven, preventing a direct comparison with the C-J pressure (Bozier et al., 2009). Moreover, the diameter of the sensor head (approximately 0.32 cm) is much smaller than the detonation cell size of CH_4-air (20 cm or more (Gamezo et al., 2012)). For detonation, the pressure at the shock front can be two times that of the C-J pressure (Bjerketvedt et al., 1997). Despite these challenges, the proposed model provides sufficient accuracy for engineering applications.

However, in the case of 5.3% CH_4-air, the capability of the numerical model deteriorated as the methane concentration approached the lower detonation limit. In this instance, the shock and flame were coupled in some locations while decoupled in others, indicating an instable detonation (Gamezo et al., 2012). But, as mentioned before, the proposed model tends to give conservative predictions when the concentration is near the detonation limit.

4.3. Hydrogen-methane-air mixture

Limited data is available for detonation in hydrogen-methane-air mixtures, and as such, a small-scale test was employed to validate the proposed model. The test took place within a 6 m long steel tube with an inner diameter of 140 mm (Porowski et al., 2013). Both ends of the tube were sealed, and 12 steel rings with an area blockage ratio of 0.4 and a distance of 420 mm were employed to obstruct the tube. The tube was filled with a stoichiometric hydrogen-methane-air mixture, with 10% CH_4 in CH_4–H_2. Ignition was initiated by a weak electric spark at one end of the tube, and the flame was accelerated to detonation by the steel rings. The initial conditions were 1 atm and 293 K.

A 2D symmetric model with 1 mm mesh was utilized to reproduce the scenario, with a total mesh number of about 0.4 million. The C-J

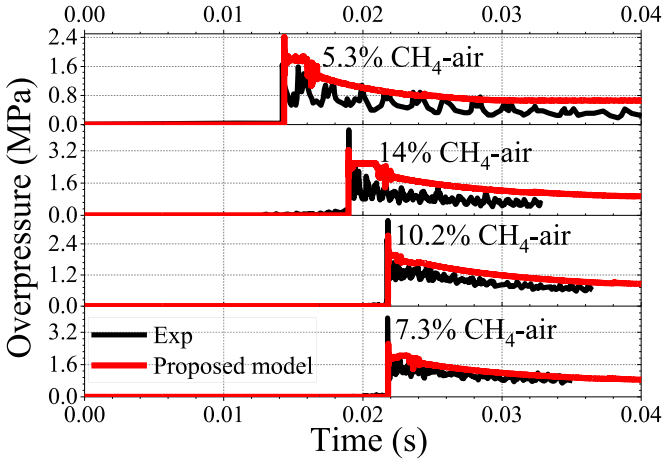

Fig. 19. Load history comparison between numerical and experimental results (Zipf et al., 2013; Gamezo et al., 2012).

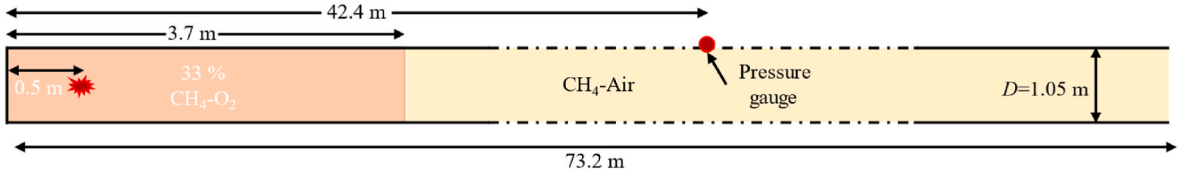

Fig. 18. Experimental setup and the gauge location.

parameters used for modelling were 0.94 kg/m^3 for density, 1919 m/s for detonation velocity, 1.64 MPa for C-J pressure, 0.166 for ω, and 5.61 MJ/m^3 for detonation energy.

Fig. 20 shows the load history comparison. For P_1, located 0.67 m away from the ignition point, the proposed model successfully captured the pressure peak. However, as the distance was not sufficient to trigger a detonation, the blast at P_1 remained a deflagration, as evidenced by the slow rise of the experimental results. However, As the flame continued to accelerate, the blast wave transitioned to a detonation wave, and the pressure history after P_3 was predicted accurately by the proposed model. Therefore, the proposed model demonstrates the capability to handle detonation, even for hydrogen-methane-air mixtures.

5. Conclusion

This study proposed a generic approach for the modelling of CH_4–H_2-air detonations within hydrocode, enabling accurate and rapid coupling of load profiles. The validity and efficiency of the proposed procedure were demonstrated against diverse experimental data and existing numerical methods.

Theoretical calculation resulted in an empirical model predicting C-J parameters for hydrocode input. The study leveraged modified open-source tools to theoretically calculate C-J parameters at equilibrium conditions, resolving the implicit coupling of detailed chemical reactions and thermodynamic properties. Key findings included: a 10% decrease in detonation velocity and an increase in C-J pressure with increasing methane concentration from 0% to 100%. As concentration increased, for pure H_2, detonation velocity rose by 36%, but in H_2–CH_4 mixtures, it initially increased until the equivalence ratio of fuel slightly above 1.1, then decreased. The maximum C-J pressures and detonation energy occurred around an equivalence ratio of 1.1, diminishing at other concentrations. The heat capacity ratio was lowest near the equivalence ratio of 1.1. Initial temperature exhibited a slight negative impact on detonation velocity and a more significant effect on C-J pressure and detonation energy. The developed empirical model covered typical industrial conditions, including standard atmospheric pressure, temperatures from −20 to 40 °C, and fuel concentrations within the detonable limit of the H_2–CH_4-air mixture.

Additionally, the study detailed the utilization of these C-J parameters in LS-DYNA hydrocode for modelling gas detonation and blast propagation. Employing a modified JWL state equation, the method effectively simulated various conditions, including H_2-air, CH_4-air, and H_2–CH_4-air mixtures, and different concentration ranges, experimental scales, boundary conditions, and fuel geometries. This approach replicated blast loading, and demonstrated over 90% computational efficiency improvement as compared to traditional CFD methods by eliminating the need for ultra-fine meshing and complex chemical-fluid coupling. This approach tended to yield conservative loading predictions when the gas detonation is unstable.

The adaptability of this method for simulating detonations in different gas mixtures extends its applicability beyond CH_4–H_2-air, rendering it a remarkable tool for modelling gas detonation phenomena, potentially enhancing safety protocols in industries like oil and gas, chemical production, transportation, and storage.

CRediT authorship contribution statement

Di Chen: Writing – review & editing, Writing – original draft, Visualization, Validation, Investigation, Formal analysis. **Jun Li:** Supervision, Resources, Methodology, Funding acquisition. **Li Wang:** Supervision, Conceptualization. **Chengqing Wu:** Conceptualization.

Declaration of generative AI and AI-assisted technologies in the writing process

Statement: During the preparation of this work the authors used ChatGPT, an AI language model in order to improve the readability and language of this work. After using this tool, the authors reviewed and edited the content as needed and take full responsibility for the content of the publication.

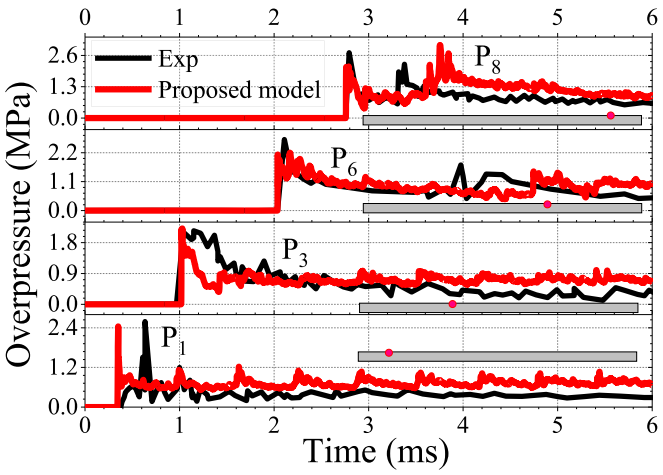

Fig. 20. Load history comparison between numerical and experimental results (Porowski et al., 2013).

Declaration of competing interest

The authors declare the following financial interests/personal relationships which may be considered as potential competing interests: Jun Li reports was provided by Australia Research Council. If there are other authors, they declare that they have no known competing financial interests or personal relationships that could have appeared to influence the work reported in this paper.

Data availability

Data will be made available on request.

Acknowledgments

This work was supported by the Australia Research Council under ARC Discovery Project DP210101100.

References

Abdelaal, H., et al., 2005. A new approach to utilize Hydrogen as a safe fuel. Int. J. Hydrogen Energy 30 (13–14), 1511–1514.
Anderson, C.E., 1987. An overview of the theory of hydrocodes. Int. J. Impact Eng. 5 (1), 33–59.
Baker, E.L., et al., 2010. Theory and calibration of JWL and JWLB thermodynamic equations of state. WIT Trans. Built Environ. 113, 147–158.
Biennial report on hydrogen safety, The International Association for Hydrogen Safety, 2007, pp. 1–318, Version 1.2.
Bjerketvedt, D., Bakke, J.R., van Wingerden, K., 1997. Gas explosion handbook. J. Hazard Mater. 52 (1), 1–150.
Bozier, O., et al., 2009. Detonability of binary H2/CH4 - air mixture. In: International Conference on Hydrogen Safety. France.
Chae, M.J., et al., 2022. The present condition and outlook for hydrogen-natural gas blending technology. Kor. J. Chem. Eng. 39 (2), 251–262.
Chapman, D.L., 1899. VI. On the rate of explosion in gases. London, Edinburgh Dublin Phil. Mag. J. Sci. 47 (284), 90–104.
Chen, Di, 2023. Gas explosion & safety. www.dichen-safe.tech/index.php/resource/.
Chen, D., et al., 2022. A numerical study of gas explosion with progressive venting in a utility tunnel. Process Saf. Environ. Protect. 162, 1124–1138.
Chen, D., et al., 2023a. An overpressure-time history model of methane-air explosion in tunnel-shape space. J. Loss Prev. Process. Ind. 82, 105004.
Chen, D., Wu, C., Li, J., 2023b. Assessment of modeling methods for predicting load resulting from hydrogen-air detonation. Process Saf. Environ. Protect. 180, 752–765.
Edwards, D.H., Williams, G.T., Breeze, J.C., 1959. Pressure and velocity measurements on detonation waves in hydrogen-oxygen mixtures. J. Fluid Mech. 6 (4), 497–517.

Gamezo, V.N., et al., 2012. Detonability of natural gas–air mixtures. Combust. Flame 159 (2), 870–881.
Goodwin, D.G., Moffat, H.K., Speth, R.L., 2023. Cantera: an Object-Oriented Software Toolkit for Chemical Kinetics, Thermodynamics, and Transport Processes.
Gordon, S., McBride, B.J., 1994. Computer program for calculation of complex chemical equilibrium compositions and applications. Part 1: Analysis, pp. 1–64.
Groethe, M., et al., 2007. Large-scale hydrogen deflagrations and detonations. Int. J. Hydrogen Energy 32 (13), 2125–2133.
Guo, Y., et al., 2016. Numerical investigation of surface conduit parallel gas pipeline explosive based on the TNT equivalent weight method. J. Loss Prev. Process. Ind. 44, 360–368.
Hao, H., et al., 2016. Review of the current practices in blast-resistant analysis and design of concrete structures. Adv. Struct. Eng. 19 (8), 1193–1223.
Hydrogen Scaling up: a Sustainable Pathway for the Global Energy Transition, 2017. Hydrogen Council.
Institute, E., 2023. Statistical Review of World Energy 2023, pp. 1–64. London.
Jin, K., et al., 2021. Effect of ignition position on premixed hydrogen-air flame quenching behaviors under action of metal wire mesh. Fuel 289, 119750.
Jouguet, E., 1905. On the propagation of chemical reactions in gases. J. Math. Pure Appl. 1 (2), 347–425.
Kao, S., et al., 2023. SDToolbox-Numerical Tools for Shock and Detonation Wave Modeling. California Institute of Technology, Pasadena, California.
Kim, D., Kim, J., 2019. Numerical method to simulate detonative combustion of hydrogen-air mixture in a containment. Engineering applications of computational fluid mechanics 13, 938–953.
Kim, S., et al., 2023. Behavior of barrier wall under hydrogen storage tank explosion with simulation and TNT equivalent weight method. Appl. Sci. 13 (6), 3744.
Kuznetsov, M., et al., 2022. Flame propagation regimes and critical conditions for flame acceleration and detonation transition for hydrogen-air mixtures at cryogenic temperatures. Int. J. Hydrogen Energy 47 (71), 30743–30756.
Lee, E.L., Horning, H.C., Kury, J.W., 1968. Adiabatic Expansion of High Explosive Detonation Products. Lawrence Radiation Laboratory, Universify of California, California.
Li, B., et al., 2019. Numerical simulation and full-scale test on dynamic response of corroded concrete pipelines under Multi-field coupling. Construct. Build. Mater. 200, 368–386.
Li, Z., et al., 2021. Gas explosions of methane-air mixtures in a large-scale tube. Fuel 285, 119239.
Liao, K., et al., 2023. Parametric study on natural gas leakage and diffusion in tunnels. J. Pipeline Syst. Eng. Pract. 14 (2).
López, E., et al., 2015. Analysis of high-pressure hydrogen and natural gas cylinders explosions through TNT equivalent method. In: Proceeding Hyceltec 2015. Iberian Symposium on Hydrogen, Fuel Cells and Advanced Batteries.
LS-DYNA® keyword user's manual volume II, Livermore Software Technology, 2021.
Machniewski, P., Molga, E., 2022. CFD analysis of large-scale hydrogen detonation and blast wave overpressure in partially confined spaces. Process Saf. Environ. Protect. 158, 537–546.
Mcbride, B.J., Gordon, S., Reno, M.A., 1993. Coefficients for Calculating Thermodynamic and Transport Properties of Individual Species, vol. 4513. National Aeronautics and Space Administration, Office of Management, Scientific and Technical Information Program.
Mueschke, N.J., Joyce, A., 2020. Measurement of gas detonation blast loads in semiconfined geometry. J. Loss Prev. Process. Ind. 63, 104004.
Nozu, T., et al., 2005. Numerical simulation of hydrogen explosion tests with a barrier wall for blast mitigation. In: Proceedings of the 1st International Conference on Hydrogen Safety. Pisa, Italy.
Oran, E.S., Gamezo, V.N., Zipf, R.K., 2015. Large-scale experiments and absolute detonability of methane/air mixtures. Combust. Sci. Technol. 187 (1–2), 324–341.
Pan, Y., et al., 2023. Experimental and numerical study on ground shock propagation in calcareous sand. Int. J. Impact Eng. 180, 104724.
Pan, Y., et al., 2024. Investigating the dynamic response of a double-box utility tunnel buried in calcareous sand against ground surface explosion. Tunn. Undergr. Space Technol. 146, 105636.
Porowski, R., Teodorczyk, A., 2013. Experimental study on DDT for hydrogen–methane–air mixtures in tube with obstacles. J. Loss Prev. Process. Ind. 26 (2), 374–379.
Rehm, W., Jahn, W., 1993. Contribution to the Investigation of Balloon Experiments for the Propagation Functions of Detonating Hydrogen-Air Mixtures with Test Examples. Forschungszentrum Juelich GmbH (Germany).
Rudy, W., Zbikowski, M., Teodorczyk, A., 2016. Detonations in hydrogen-methane-air mixtures in semi confined flat channels. Energy 116, 1479–1483.
Smith, G.P., 2000. http://combustion.berkeley.edu/gri-mech/version30/text30.html.
Souli, M., et al., 2004. ALE and fluid structure interaction in LS-DYNA. In: 8th International LS-DYNA Conference. Detroit.
Stamps, D.W., Slezak, S.E., Tieszen, S.R., 2006. Observations of the cellular structure of fuel–air detonations. Combust. Flame 144 (1), 289–298.
Sun, S., et al., 2020. Effects of concentration and initial turbulence on the vented explosion characteristics of methane-air mixtures. Fuel 267, 117103.
van den Berg, A.C., 1985. The multi-energy method: a framework for vapour cloud explosion blast prediction. J. Hazard Mater. 12 (1), 1–10.
Van den Berg, A.C., Lannoy, A., 1993. Methods for vapour cloud explosion blast modelling. J. Hazard Mater. 34 (2), 151–171.
Wang, J., et al., 2009. Numerical study of the effect of hydrogen addition on methane–air mixtures combustion. Int. J. Hydrogen Energy 34 (2), 1084–1096.
Weng, Z., Mével, R., 2022. Real gas effect on steady planar detonation and uncertainty quantification. Combust. Flame 245, 112318.
White, F.M., 1990. Fluid Mechanics, fourth ed. New York.
Xing, H., et al., 2020. Visualization of explosion characteristics of methane-air mixtures with different ignition positions and vent areas in a large-scale venting chamber. Fuel 279, 118380.
Yáñez, J., et al., 2011a. A comparison exercise on the CFD detonation simulation in large-scale confined volumes. Int. J. Hydrogen Energy 36 (3), 2613–2619.
Yáñez, J., et al., 2011b. A comparison exercise on the CFD detonation simulation in large-scale confined volumes. Int. J. Hydrogen Energy 36 (3), 2613–2619.
Yang, H., et al., 2016. Confined vapor explosion in Kaohsiung City – a detailed analysis of the tragedy in the harbor city. J. Loss Prev. Process. Ind. 41, 107–120.
Zbikowski, M., Makarov, D., Molkov, V., 2010. Numerical simulations of large-scale detonation tests in the RUT facility by the LES model. J. Hazard Mater. 181 (1–3), 949–956.
Zhang, B., et al., 2014. Pressure characteristics and dynamic response of coal mine refuge chamber with underground gas explosion. J. Loss Prev. Process. Ind. 30, 37–46.
Zhang, B.Y., Li, H.H., Wang, W., 2015. Numerical study of dynamic response and failure analysis of spherical storage tanks under external blast loading. J. Loss Prev. Process. Ind. 34, 209–217.
Zhang, H., et al., 2019. Numerical study of the detonation benchmark using GASFLOW-MPI. In: International Conference on Hydrogen Safety. Germany.
Zhang, S., et al., 2020. Numerical simulation on methane-hydrogen explosion in gas compartment in utility tunnel. Process Saf. Environ. Protect. 140, 100–110.
Zhu, Y., et al., 2015. Analysis and assessment of the Qingdao crude oil vapor explosion accident: lessons learnt. J. Loss Prev. Process. Ind. 33, 289–303.
Zipf, R.K., et al., 2013. Methane–air detonation experiments at NIOSH lake lynn laboratory. J. Loss Prev. Process. Ind. 26 (2), 295–301.